16th ICAAR LISBOA 2020-2022

16th International Conference on
Alkali-Aggregate Reaction in Concrete
Lisboa | LNEC | Portugal | 31 May - 2 June 2022

http://icaar2020-2022.lnec.pt

Alkali silica reaction – sequence, products and possible mechanisms of expansion

Andreas Leemann (1)

(1) *Empa, Dübendorf, Switzerland, andreas.leemann@empa.ch*

Abstract

Although alkali silica reaction is the focus of research since decades, many open questions remain. This paper addresses some of these open questions and focuses on the sequence of reaction and the type of reaction products formed, including their composition and structure.

***Keywords**: alkali-silica reaction, composition, sequence, structure.*

1. INTRODUCTION

Alkali silica reaction (ASR) can lead to considerable damages of concrete structures. Although the worldwide occurring phenomenon is in the focus of research since decades, many open questions remain. According to a simplified description, the alkaline pore solution of the concrete dissolves SiO_2 from metastable minerals in aggregates, leading to the formation of ASR products. This process goes together with stress generation in aggregates, eventually leading to crack formation and concrete damage. In spite of their significant effect on deformation and crack formation of concrete, the volumes of ASR products formed are relatively small. This poses a major challenge for studying ASR. Firstly, the sequence of reaction is difficult to follow, in particular in the stage before initial cracking occurs. At this stage, the size of the ASR products is in the micrometre to sub-micrometre range. Secondly, the typical methods to characterize bulk samples of hydrates are usually not applicable, as the amounts extractable from aggregates are in the range of a few micrograms at best. However, detailed knowledge on the sequence of reaction and an in-depth characterisation of the ASR products are the basis to improve the understanding of ASR and of the mechanism leading to expansion and stress generation.

In the following, the current knowledge about the sequence of reaction and about the ASR products are given, relying mainly on published and in some special cases on unpublished data.

2. MATERIALS AND METHODS

The information on materials and methods used is given in the corresponding references. Detailed information is only given for the data that have not been published previously.

All the elemental ratios given are based on atom-%.

Figure 3.1 is an illustration of the reaction sequence based on the image analysis of an aggregate in a caesium (Cs)-doped concrete at the age of eight weeks studied in [1]. Figure 3.2A shows the back-scattering image and Figure 3.2D the segmentation thereof. The other images in the sequence are illustrations.

Figures 4.6 and 4.7 have been acquired on broken surfaces of a concrete from a bridge (4.6A), a concrete prism tested at 38 °C (4.6B), a concrete prism tested at 60 °C (11A) and a synthesized powder sample (4.7B). More information on the specific samples can be found in [2-4]. A scanning electron microscope (SEM, FEI Quanta 650) at a pressure of 3.0-4.5 × 10^{-6} Torr was used with a Everhart-Thornley detector for secondary (SE)-image acquisition. Settings depended on the particular problem to be investigated. Therefore, a relatively wide range of acceleration voltage (2-12 kV) and spot size (1.5-4.5) were used. The samples were carbon coated. Information on the SEM settings for the back-scattering images and energy-dispersive X-ray spectroscopy is given in the referenced papers. All composition are given as atom-% or ratios thereof.

For studying the response of amorphous and crystalline ASR products to changes in relative humidity (RH, see paragraphs 5.3 and 5.4) one aggregate was split along a vein containing ASR products and stored in an airtight box. Another concrete sample containing an aggregate with a vein filled with crystalline ASR product was ground and again stored in an airtight box. In both cases, the mass of the samples was ~ 1 g. They were stored in a container with a volume of 5 ml that additionally contained 1

g of portlandite wrapped in paper to serve as CO_2 sink. RH at the time of closing the containers was ~ 60 %. Two days later, the two samples were studied in an FEI Quanta 650 using the environmental SEM mode and a gaseous analytical solid-state, back-scattered electron (GAS) detector. The samples were installed on a Peltier stage cooled to a temperature of 4 °C. The targeted RH for the start of the experiment was the crystalline ASR product ~ 50 % in the case of the amorphous product and ~ 40 % for the crystalline product, respectively. RH was increased up to the saturation point by pressure adjustments. Pressure was increased at 0.1 mbar/min. After an increase of 1 mbar, the pressure was kept constant for 15 minutes, then the pressure was increase again stepwise by 1 mbar. After reaching the saturation point, the pressure was decreased to reach ~ 90 % RH, where it was kept constant for 1.5 hours for the amorphous ASR product. The same was done for the crystalline ASR product, but the RH was kept at ~ 95 % RH for 1.5 hours. Afterwards, the experiment with the crystalline ASR product was terminated. The amorphous product was stored at close to 97 % RH in a desiccator flooded with N_2 for 24 h and investigated again. Applied pressure was between 3 and 9 mbar. Images were taken at the different RH conditions.

3. REACTION SEQUENCE

In order for ASR products to be formed, SiO_2 has to be dissolved first. The kinetics of SiO_2 dissolution in an alkaline environment depends mainly on the degree of crystallinity. Amorphous SiO_2, as present in chert or volcanite, is the most reactive phase and a perfectly crystalline quartz the least reactive one. The process of dissolution under varying boundary conditions is described in various papers [5-13] and summarized in [14]. The influence of specific ions on SiO_2 dissolution in the alkaline environment representative for the pore solution of concrete is targeted in [15]. It can be assumed that SiO_2 dissolution in the aggregates occurs wherever the existing porosity allows contact of reactive minerals with the pore solution of the concrete. However, the formation of ASR products starts in inherent, pre-existing porosity of the aggregate directly adjacent to the cement paste [16-21]. In Swiss aggregates, this inherent porosity is typically in the range of 0.5-1.0 volume-% (determined according to EN 1097-6, unpublished data). The first ASR products are difficult to observe in the SEM, as they are present mostly in the micrometre and sub-micrometre range, making an analysis by EDS difficult. An accurate analysis of these products is only possible by cutting lamellas with a focused ion beam (FIB) and subsequent analysis in a transmission electron microscope (TEM) as performed in [22, 23]. This approach not only allows the chemical analysis of ASR products. Selected area electron diffraction (SAED) permits to distinguish between amorphous and crystalline phases. In addition to the difficulties in the chemical analysis of these initial ASR products formed in the pre-cracking state, their backscattering contrast is in the same range as the one of quartz, not allowing to visually distinguish them from the aggregate. However, this situation can be changed using Cs as a tracer [21]. $CsNO_3$ can be added to the mixing water of concrete. As an earth alkali, it is bound in the ASR products. Due to its higher atomic number compared to Si, Na, K, Ca and O, it significantly enhances backscattering contrast and makes ASR products easily recognisable in the SEM (Figure 3.1). As such, it allows to follow the sequence of reaction with a resolution down to the sub-micrometre scale.

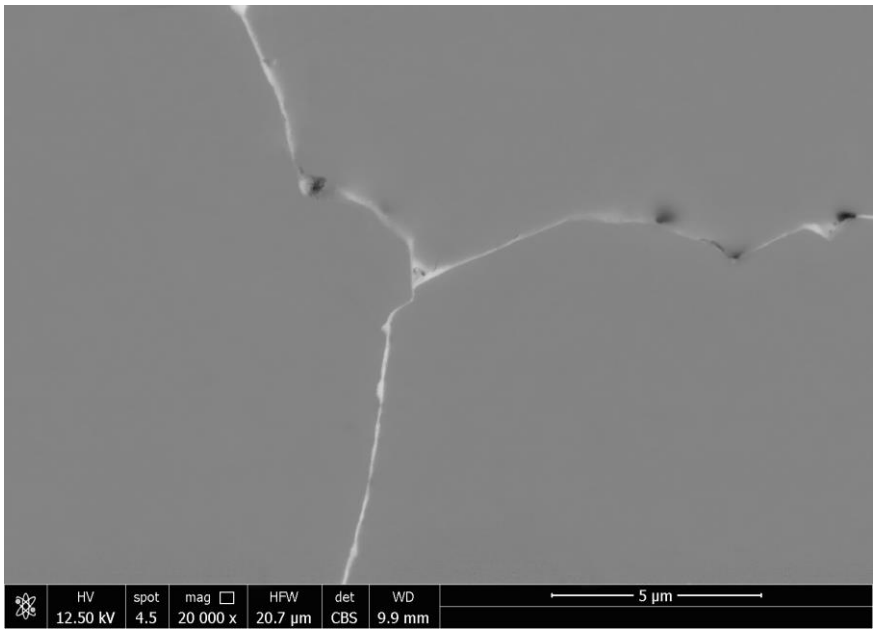

Figure 3.1: Thin layers of ASR products with a thickness well below one micrometre are located between adjacent quartz grains in an uncracked aggregate of a Cs-doped concrete. The ASR products stand out due to the increased backscattering contrast caused by the presence of Cs. Horizontal field width (HFW) = 20.7 µm. Image from [1].

In the Cs-doped concrete, the reaction sequence (described in more detail in [21]) can be observed as follows. ASR products start to form close to the interface with the cement paste in the pre-existing porosity of the aggregate. ASR product formation continuously progress towards the interior of the aggregate as a front. The formation of these small volumes of products is obviously linked to the generation of stress, as the majority of aggregates showing their formation crack. However, the point of cracking shows no direct relation to the depth the front has reached in aggregates. Some aggregates crack, although the front has progressed only to a depth of a few hundred micrometres. Some aggregates have not cracked yet, in spite of the fact that the front has reached their centre. If a reactive aggregate cracks and when it cracks is likely dependent on its mechanical properties.

When cracks start to extend from aggregate to paste, there is an immediate extrusion or diffusion of ASR products into the cement paste. Here, two different situations are observed. In the first, the aggregate develops multiple cracks that do not proceed into the cement paste. In this situation, the ASR products only advance into the porosity of the cement paste adjacent to the aggregates. In the second situation, the aggregates form a major crack running into the cement paste. Here, the ASR products and highly concentrated alkali-silica sol/gel are extruded into the crack reaching distances from the aggregate of several millimetres. In both cases, relatively little ASR product remains in the areas of the aggregates connected to the formed cracks. Typically, the cracks in the aggregates are empty and ASR product only remains in the crack close to the interface with the cement paste forming a plug. An illustration of this sequence of reaction is shown in Figure 3.2.

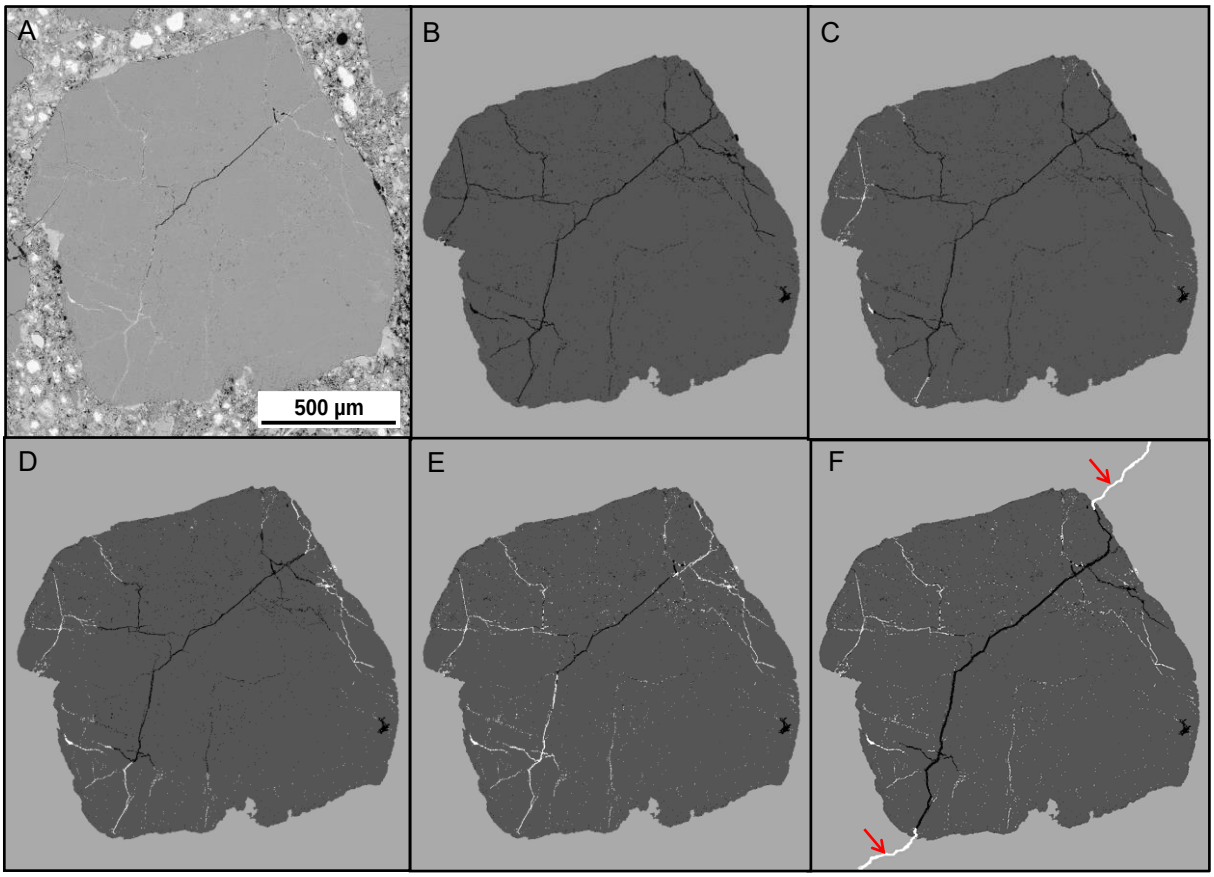

Figure 3.2: Illustration of the reaction sequence based on a quartzite aggregate in an eight week-old Cs-doped concrete (A). It shows the aggregate before reaction with the pre-existing porosity in black (B), the ongoing reaction with the ingress of ASR products (C-E) and the point of cracking with the immediate extrusion of ASR products into the cement paste along the newly formed crack (red arrows) and the depletion of ASR products in the regions of the aggregate connected with the crack (F).

Cs is not only able to increase the backscattering contrast in the SEM, but increases as well the X-ray attenuation due to its high atomic number. Using X-ray micro-tomography (XMT), it is possible to observe not only the crack formation but as well the formation of ASR products [24]. As XTM is non-destructive, it allows to follow the progress of ASR on the same samples, time-resolved and in 3D.

After cracking, the practically empty cracks in the aggregates start to fill with ASR products. This filling starts from the typical plug of amorphous ASR products close to the interface to the cement paste. However, crystalline ASR products are formed predominately at this stage. A representative example is shown in Figure 3.3.

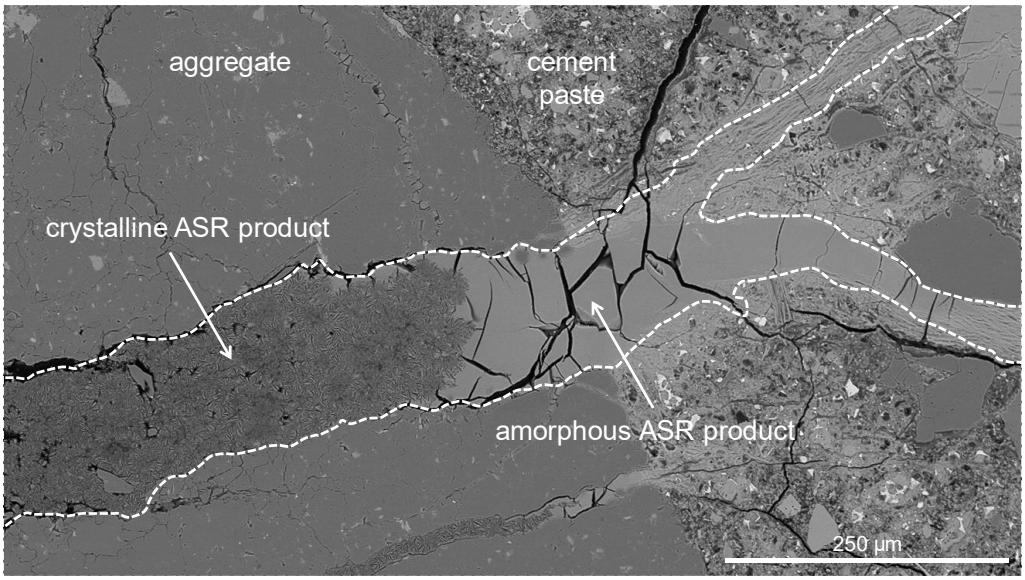

Figure 3.3: Typical spatial distribution of amorphous and crystalline ASR product filling a crack extending from the aggregate into the cement paste. Laboratory produced concrete tested with the concrete prism test (CPT) at 38 °C.

This situation is not only typical for slow reacting types of aggregates like sandstone, gneiss, granite or quartzite. It occurs as well in the case of fast reacting aggregates like chert (Figure 3.4). The plug close to the interface and the products extruded into the cement paste consist of amorphous ASR products and the ones formed in the aggregate after initial cracking are predominantly crystalline.

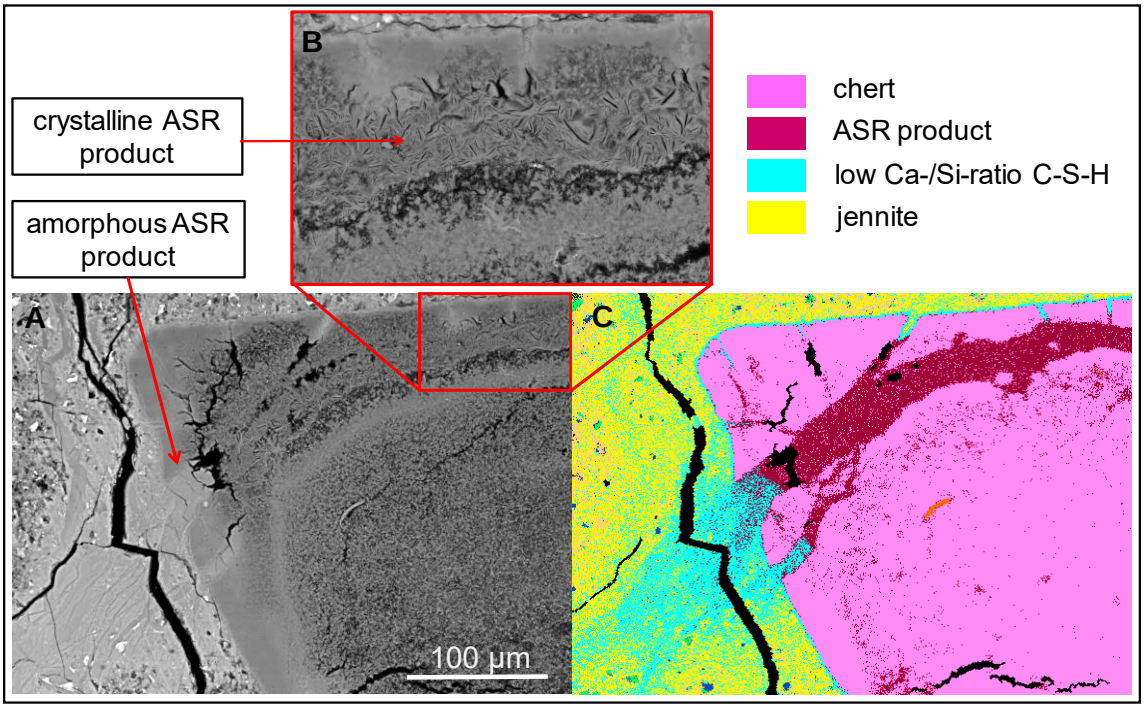

Figure 3.4: Cracked chert particle containing amorphous and crystalline ASR products (A) with a location showing crystalline ASR products enlarged for better visibility (B). Phase map based on element maps showing chert, ASR products, extruded amorphous ASR products converted to low Ca/Si-ratio calcium-silicate-hydrate (C-S-H) and the matrix of regular C-S-H ("jennite"). 14 year old concrete from an exposure site. Clustering performed according to the method published in [25].

4. REACTION PRODUCTS

4.1 Composition

The initial ASR products formed are amorphous [4, 21]. At an early stage of the reaction, their composition varies with their location in the aggregates and it evolves with time. The ASR products present at the head of the ingressing reaction front with greater distance to the cement paste display a lower Ca/Si-ratio than the ones closer the periphery of the aggregate [21]. However, when the reaction front has reached the centre of the aggregates, these differences are balanced by the Ca uptake of the products with initially low Ca/Si-ratio. As a result, the mean Ca/Si-ratio of the ASR products at an early stage is lower than at a later stage. This can be seen in Figure 4.1, where the number of points with low Ca/Si-ratio decreases going from 4 (not shown) to 8 to 24 weeks. The corresponding mean values of the Ca/Si-ratio are 0.12, 0.18 and 0.21, respectively. However, it is interesting to note that there seems to be an upper limit of the Ca/Si-ratio at a value of ~ 0.35. This could indicate that the Ca uptake of the amorphous ASR products reaches a stable level in the chemical environment present inside of aggregates. Only at the interface with the cement paste a higher Ca uptake is possible, as described later. On the other hand, the ASR products with a very low Ca/Si-ratio (approximately < 0.05) may be simply an artefact of sample preparation. In the parts of the aggregate not yet reached by the inward diffusion of Ca, an alkali-silicate sol at or close to saturation can be expected to be present. When the sample is dried prior to epoxy impregnation, the loss of water leads to supersaturation and the precipitation of alkali-silicate-hydrates. These precipitates are measured with EDS later and are included in Figure 4.1, although at least some of them may not have formed without sample drying.

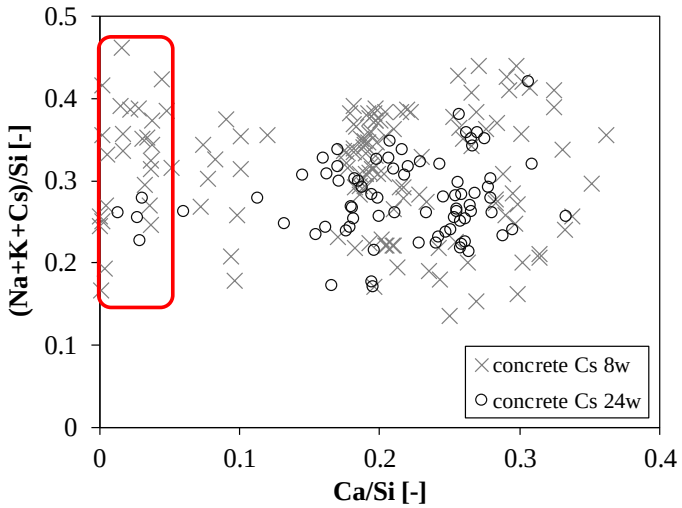

Figure 4.1: (Na+K+Cs)/Si-ratio as a function of Ca/Si ratio of amorphous ASR products formed in aggregates of a Cs-doped concrete tested with the CPT at 60 °C at the age of 8 and 24 weeks. The red rectangle indicates ASR products with a Ca/Si-ratio < 0.05 that may have precipitated due to sample drying prior to epoxy impregnation.

There are differences in the composition of amorphous and crystalline ASR products formed in aggregates as an in-depth analysis has shown [4]. Although the mean values for Ca/Si-ratio and (Na/K)/Ca-ratio are very similar (Figure 4.2), the Ca/Si-ratio of the amorphous products varies more. Additionally, they exhibit a higher Na/K-ratio than the crystalline ones (Figure 4.3). These data are based on the concrete tested with the CPT at 38 and 60 °C using two different types of aggregates. A corresponding analysis of concrete from structures with several hundreds of EDS point analysis has not been conducted yet.

A possible reason for the differences in the Na/K-ratio between amorphous and crystalline ASR products could be the kinetics of gelation and formation of crystalline products as discussed in [4]. In the presence of Ca, a Na-silicate sol gels faster than a K-silicate sol [26]. The preference for Na in gelation is shown as well by the gels synthesized in [4]. On the other hand, crystalline ASR products synthesized at 40 °C seem to form faster in a K-system than in a Na-system [27]. This applies to concrete without boosting.

Boosting with either NaOH and KOH significantly affects the composition of the products formed [28, 29].

The amorphous ASR products extruded into the cement paste take up Ca and release alkalis. This process has been described in various papers [18, 19, 30-35]. Due to this alteration, they are not representative anymore for the ASR products that have caused expansion and cracking.

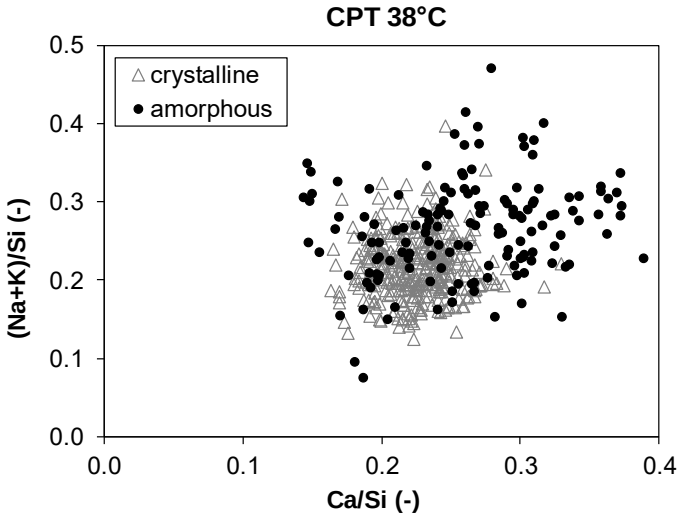

Figure 4.2: (Na+K)/Si-ratio as a function of Ca/Si-ratio of crystalline and amorphous ASR-products formed in aggregates of a concrete tested at 38 °C. Data redrawn from [4].

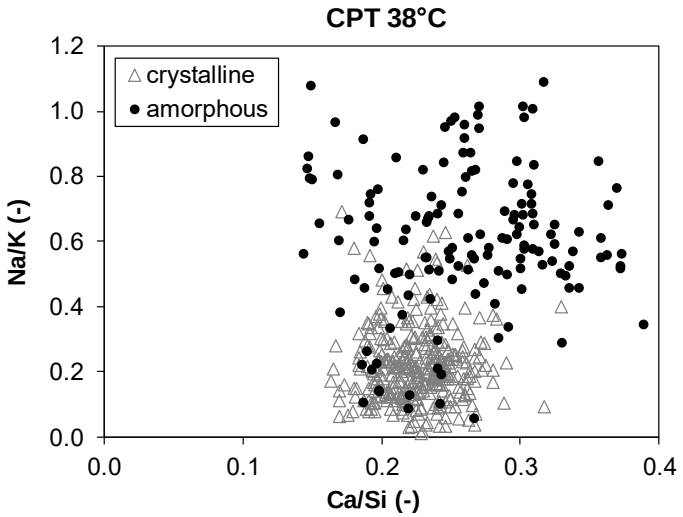

Figure 4.3: Na+K-ratio as a function of Ca/Si-ratio of crystalline and amorphous ASR-products formed in aggregates of a concrete tested at 38 °C. Data redrawn from [4].

4.2 Structure

So far, little is known about the structure of amorphous ASR products. A few attempts have been made to gain structural information from samples collected from the concrete surface of a dam applying several different methods [36-38]. However, as these samples are not directly collected from the interior of aggregates and are possibly altered by their contact to the cement paste and by carbonation, they are likely not representative of the initial ASR product leading to cracking of aggregates. The acquisition of Raman spectra in the transition from crystalline to amorphous ASR products and at the edge of aggregates has shown that amorphous ASR product seem to have bands attributable to Q^2 sites (Si-tetrahedra with two bridging oxygen atoms typical for a chain structure) and Q^3 sites (Si-tetrahedra with three bridging oxygen atoms typical for a layer structure) [39, 40]. However, these spectra represent a mixture of crystalline and amorphous ASR products. Following the vein of ASR products further into the cement paste, the intensity of the Q^2-band increases and the one of the Q^3-band decreases [39, 40].

The spectra pf the extruded ASR products approach the ones typical for low Ca/Si-ratio C-S-H [3, 41]. This is in agreement with their Ca uptake measured by EDS. In a recent study, Raman spectra of amorphous ASR products present in aggregates at a distance to the interface > 100 µm were successfully acquired [4]. Due to their distance to the interface, they can be regarded as representative for the initial ASR product leading to aggregate cracking. They exhibit distinct bands of Q^2 and Q^3 sites in the bending vibration range (~658 and ~606 cm^{-1}, respectively) with a weak band of Q^2 sites and strong one of Q^3 sites in the stretching vibration range (~1020-1030 and ~1078 cm^{-1}, respectively) as shown in Figure 4.4. Synthesized amorphous ASR products with similar Ca/Si- and (Na+K)/Si-ratio exhibit very similar Raman spectra (Figure 4.4). Nuclear magnetic resonance (NMR) performed on the synthesized products confirms the designation of the bands [4].

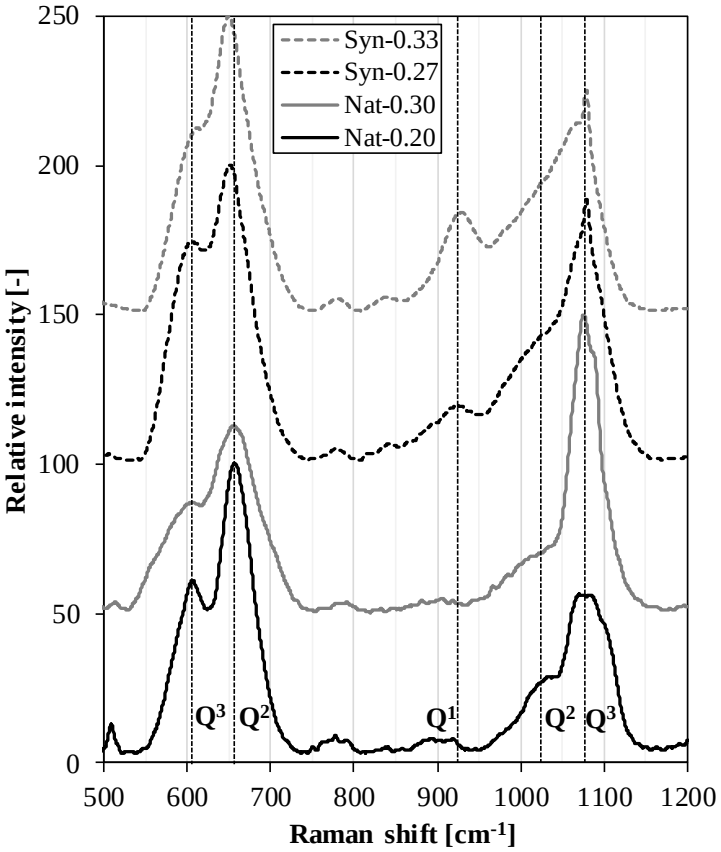

Figure 4.4: Raman spectra with band designations to Q^1, Q^2 and Q^3 sites of amorphous ASR products formed in aggregates ("Nat") and synthesized ASR products ("Syn"). The numbers given with the sample name refer to the Ca/Si-ratio of the products. Figure redrawn from [4].

Relatively large amounts of crystalline ASR products are formed in a second stage of the reaction after the initial cracking of the aggregates. It is not entirely clear, if they can already form before cracking. At least, they are usually only observable in the SEM afterwards. Most of the time, they are tightly packed in veins of aggregates. When observed in the SEM, the orientation of shrinkage cracks caused by drying during sample preparation seems to indicate that the crystalline ASR products form stacks of platelets (Figure 4.5). When their growth is not restricted by a limitation of space, they are able to display their idiomorphic form as platelets (Figure 4.6).

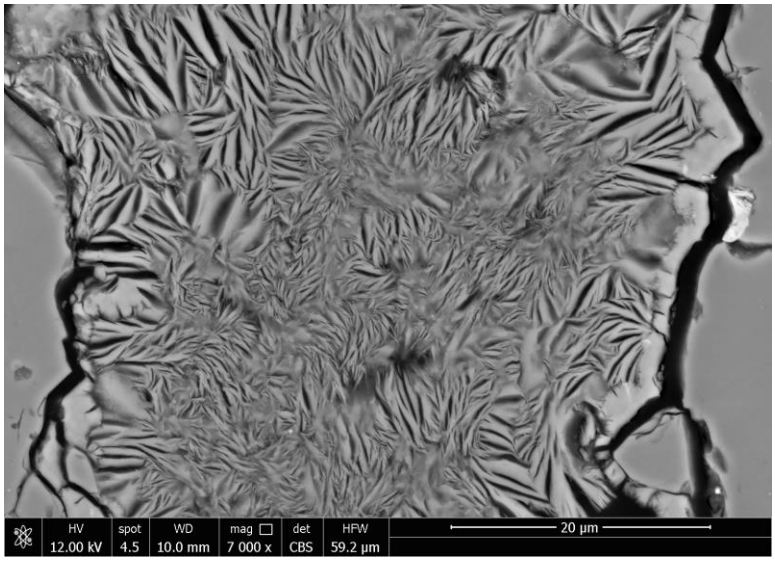

Figure 4.5: Tightly packed crystalline ASR products in the vein of an aggregate. Sample from CPT at 38 °C. HFW = 59.2 µm.

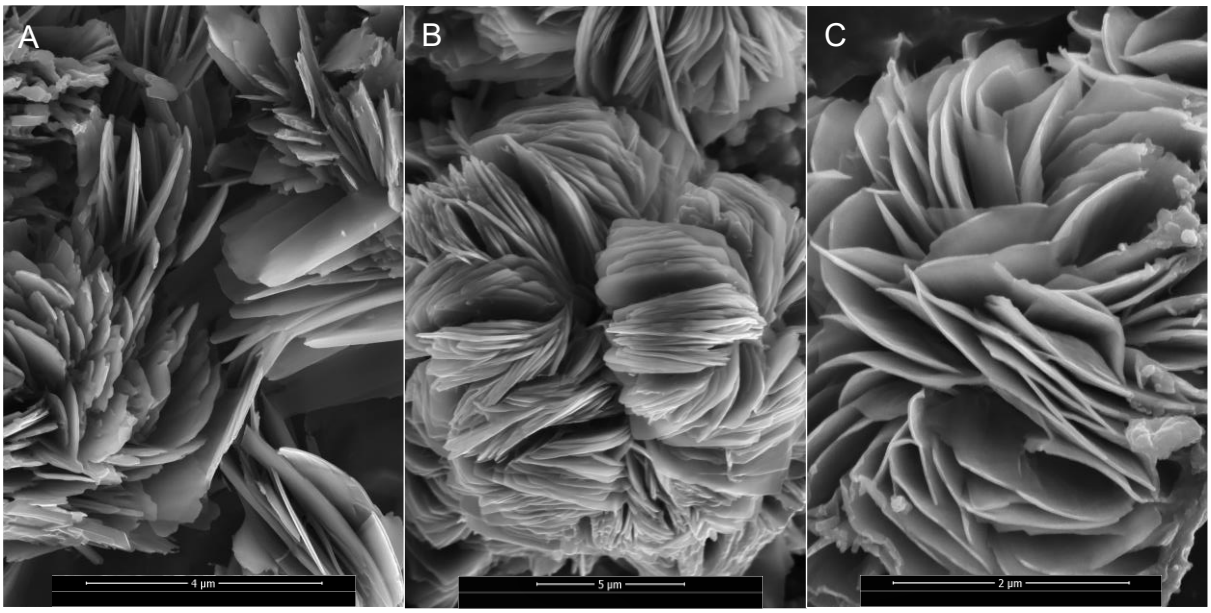

Figure 4.6: Crystalline ASR products formed in a bridge (A) and in the CPT at 38 °C (B) and synthesized at 40 °C (C, [27]). Vertical field width (VFW) = 10.4 (A), 20.7 µm (B) and 5.2 µm (C).

Crystalline ASR products present in field-exposed concrete of various mix designs have similar structure as indicated by Raman microscopy [39-41]. The Raman spectra are dominated by a band attributable to Q^3 sites with a secondary band attributable to Q^2 sites, both in the bending and in the stretching vibration range (Figure 4.7). This is clearly indicative for a layer silicate. Moreover, the Raman spectra of crystalline products formed in the CPT at 38 °C are identical to the ones formed in concrete structures. However, crystalline ASR products formed in the CPT at 60 °C display a different spectrum [3,4,39,41]. Here, the recent advances in the synthesis of crystalline ASR products prove to be decisive for further advances in the knowledge about ASR [3, 27]. The Raman spectra of crystalline ASR products synthesized at 20 and 40 °C are identical to the ones formed in field-exposed concrete, while the ones of crystalline ASR products synthesized at 80 °C are identical to the ones formed in the CPT at 60 °C and the accelerated mortar bar test at 80 °C [4, 28, 40]. This clearly shows that the type of product formed is dependent on temperature. The mineral formed at higher temperature is the mineral shlykovite. The synthesis resulted in pure Na- and pure K-shlykovite depending on the types of boosting alkalis [3]. Formation of K-shlykovite has been identified in field-exposed concrete from an outdoor

exposure site in Valencia/Spain [42, 43], where it is likely that the concrete reaches temperatures above 60 °C due to solar radiation. The only other occurrence may have been in a Naval dry dock in Charleston SC, where a phase with a d-value of 13.2 Å was reported [43].

Although Raman microscopy is a powerful tool to acquire information on the structure of hydrates and minerals, X-ray diffraction (XRD) can provide more information on crystalline phases. The challenge is to extract sufficient amounts of ASR products to enable XRD. Crystalline ASR products have been analysed by XRD in various studies [44-55]. Some of the results are in general agreement to each other, while others disagree. In two recent studies, three different crystalline phases were identified in field-exposed concrete, named according to their d-spacing as 10.8 (Figure 4.6B and 4.6C), 12.3 (Figure 4.6A) and 13.4 Å phases [43, 56]. Here again, the synthesized crystalline ASR products are essential for a further classification [3, 27]. The 13.4 Å phase is identified as K-shlykovite [43]. It confirms the results of Raman microscopy that indicated this phase in concrete exposed at the site in Valencia, Spain. The 10.8 Å phase matches the XRD pattern of crystalline ASR product synthesized at 40 °C (Figure 4.6C) and the 12.3 Å phase the one synthesized at 20 °C. It has to been noted that the 10.8 and the 12.3 Å phases display identical Raman spectra indicating a limitation of the method. Some studies have reported one or two of the three phase. However, no connection between crystal structure and temperature was established [44, 45, 48, 54]. First attempts have been made to resolve the structure of the 10.8 and 12.3 Å phases based on the XRD data [27, 53, 54].

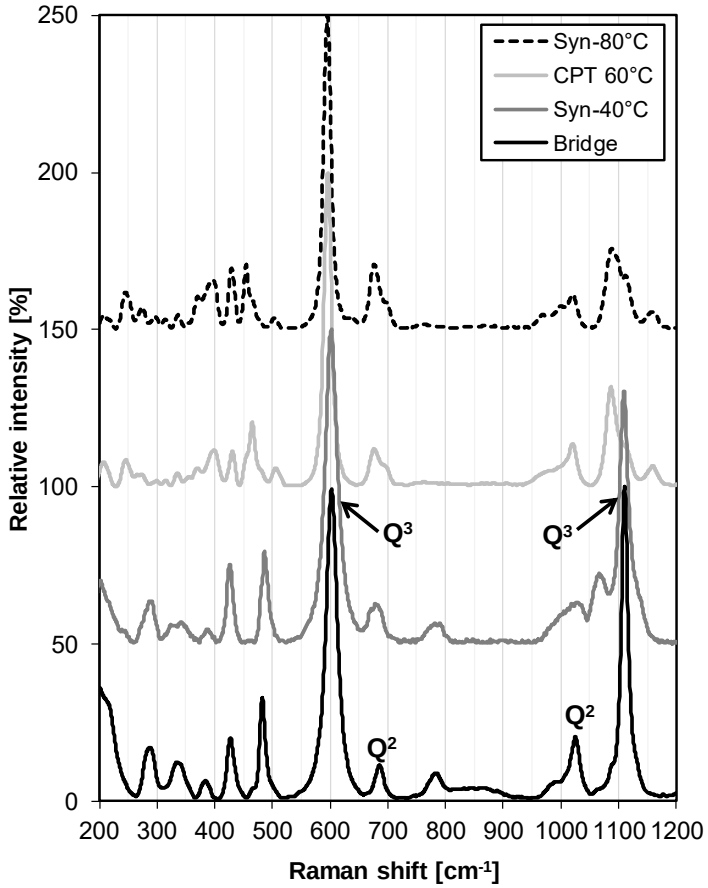

Figure 4.7: Raman spectra with band designation to Q^1, Q^2 and Q^3 sites of crystalline ASR products formed in aggregates of a bridge (d-spacing of 12.3 C), synthesized at 40 °C (d-spacing of 10.8 Å), formed in an aggregate in the CPT at 60 °C (d-spacing of 13.4 Å) and synthesized at 80 °C (d-spacing of 13.4 Å). Data adapted from [3, 4, 27, 39].

5. POSSIBLE MECHANISMS OF EXPANSION

5.1 General comment

Different hypotheses on the mechanisms of expansion in ASR-affected concrete have been proposed. The major ones are summarized in [57] and more recent ones are mentioned in [14]. It is clear from microstructural observations that the stress is generated within the aggregates, rather than in the cement paste. In principle, possible reasons for stress generation by ASR products can be divided into swelling by water imbibition in general, osmotic swelling, crystallization pressure and mass accumulation in the aggregate or any combination thereof. There are no recent results that would allow to identify the mechanism of expansion. Therefore, it seems inappropriate to come up with further speculations. However, three different aspects of ASR based on experimental data will be discussed in the following. They may help to advance the understanding on the mechanisms expansion.

5.2 Ion movement

An important aspect in ASR is the diffusion of ions and molecules. The sequence of reaction in the pre-cracking state of the aggregates discussed before gives some important information. Formation of ASR products start in the aggregate close to the interface with the cement paste [16-21]. This is due to the gradients in pH, dissolved silica, alkalis and calcium present there, as shown by reactive-transport calculations [20]. As described before, ASR products move as a front towards the interior of the aggregates. Here, a slightly adapted extraction from [21] is cited (number of references adjusted to fit the ones of the current paper):

> *Consequently, sodium, potassium, caesium and calcium have to diffuse from the cement paste to the head of the reaction front by passing the already-formed ASR products. Such diffusion must be driven by a concentration gradient of these ions between the cement paste and the aggregate generated by ASR product formation. Alkali and calcium are bound in similar quantities within the ASR products formed in concrete aggregates [2,17,18,30,31,33]. However, the calcium concentration in the pore solution of the cement paste is considerably lower compared to the one of the alkalis [58,59]. Consequently, the availability of calcium in reacting aggregates is restricted compared to the more abundant alkalis and calcium has to diffuse from the cement paste into the aggregates. Moreover, if a saturated alkali-silica solution is present in aggregates, the inward diffusion of calcium ions leads to supersaturation of this solution with respect to alkali silicates and the precipitation of ASR products as shown experimentally and by thermodynamic modelling [60]. Therefore, it can be stated that the limiting factor for the formation of the ASR products at the ingressing front is the inward diffusion of calcium leading to supersaturation. This is supported by the low Ca/Si-ratio of the ASR products as it is observed directly at the head of the ingressing front.*

These observations make it clear that ion transport along narrow gaps and pores (nanometre to a few micrometres scale at the most) plays an essential role in ASR. Moreover, it has to be taken into account that the surfaces of aggregate minerals and of the already precipitated ASR products are charged impacting both cation and anion diffusion. Reactive transport modelling may help to better understand these complex interactions in the future. The importance of transport along charged surfaces is underlined by the observation that in pre-existing cracks of aggregates with a width of several micrometres and more, C-S-H and not ASR products are formed.

5.3 Swelling of amorphous ASR products

Volume changes of amorphous ASR products have been studied at varying RH in an ESEM. The information on these experiments are given in paragraph 2. A location in the split aggregate showing both amorphous and crystalline ASR products was chosen for analysis (Figure 5.1A). The amorphous ASR product forms a layer with a thickness of about 10 µm on the crack flank of the aggregate exhibiting shrinkage cracks. Obviously, the storage in the airtight container after extracting the sample still led to drying causing these shrinkage cracks. With increasing RH, the crack width showed small changes. This is most evident after the water condensation point was reached and RH was decreased back to ~ 90 % (Figure 5.1B). Comparing Figure 5.1A and 5.1B, it is clear in some locations that the amorphous ASR product has been swelling leading to a decrease of crack width. An analysis of the dimensions of the slabs of amorphous ASR product confined by cracks indicates a swelling in X-Y-direction of about 1.2 %. However, the cracks did not close. Because it was not clear, whether the amorphous ASR

products had time to equilibrate with the RH of the chamber during the experiment, they where stored at 97 % RH for two weeks in N_2 atmosphere afterwards. However, the crack width did not change anymore as subsequent analysis showed. The drying of the amorphous ASR product seems to lead to shrinkage irreversible by rewetting. Anyway, the potential for water uptake of the amorphous ASR products seems to be limited: synthetic amorphous ASR product can have a lower water vapour sorption capacity than synthetic C-S-H [3].

Obviously, it is challenging to study the swelling of amorphous ASR products formed in concrete aggregates experimentally. In some studies, synthesized amorphous ASR products have been used for this purpose, as discussed in the following.

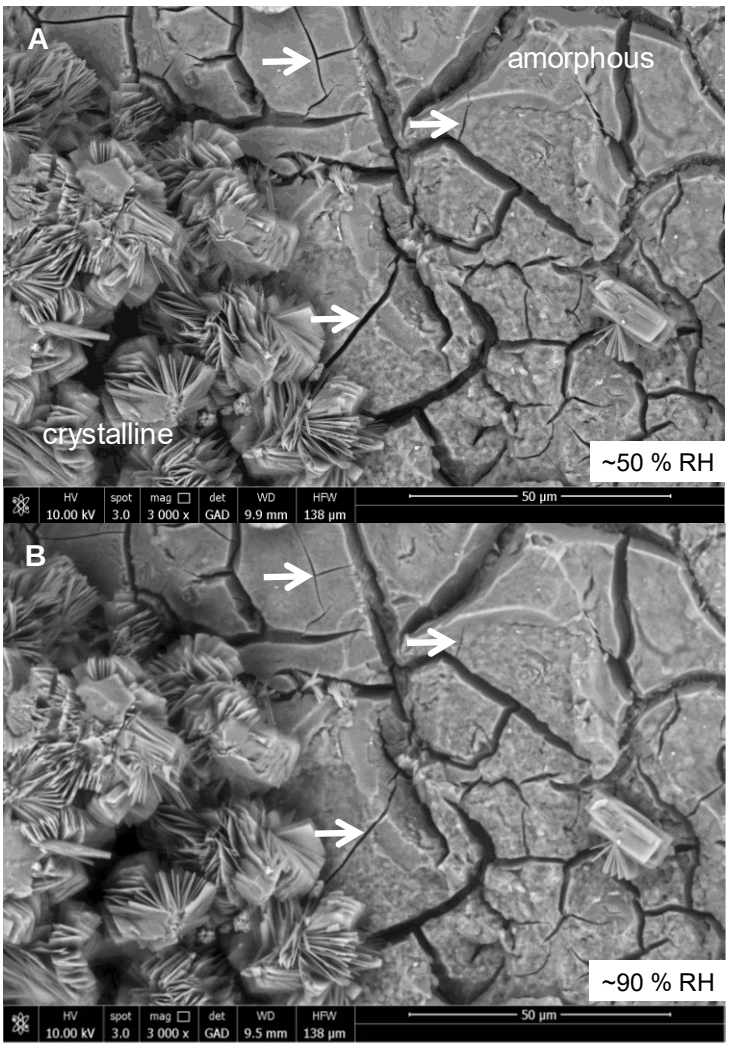

Figure 5.1: Crystalline ASR product and cracked amorphous ASR product lining a crack wall inside an aggregate in the ESEM at ~50 (A) and ~90 (B) % RH. Figure 5.1A shows the sample at the beginning of the experiment before adsorption and Figure 5.1B was made on the desorption path after reaching the point of water condensation. The white arrows indicate locations with differences in crack width. HFW = 138 µm.

In [61] the water vapour sorption of Ca-free and Ca-containing (Ca/Si-ratio of 0.03-0.32) Na- and K-based (alkali/Si-ratio of 0.29-0.40) amorphous ASR products were determined. Based on the water vapour sorption, the swelling pressure was calculated. The Ca-free product sorb substantial amounts of water vapour going from 60 to 97 % RH (up to 200 mass-%). Consequently, they show a swelling pressure according to the calculations performed. However, the products liquefied at 97 % RH. The Ca-containing products sorbed less water vapour and remained solid at 97% RH. However, the calculations did not indicate the occurrence of a swelling pressure.

In [62], free swelling and swelling pressure were determined on synthesized Na-silicates (Na/Si-ratio of 0.27-0.53) with two out of ten samples containing Ca (Ca/Si-ratio of 0.17 and 0.18). Unfortunately, [62] does not state whether the gel samples were conditioned at a certain RH before the start of the experiments. Both free swelling and swelling pressure were recorded due to water uptake of the samples. However, the amount of free swelling was not related to swelling pressure. Moreover, the swelling occurred due to uptake of water. If amorphous ASR products swell in concrete, it would be due to the uptake of alkaline pore solution and not water. Therefore, it seems that these experiments are not directly related to the chemical environment present in concrete.

The swelling behaviour of synthesized ASR products with a wide range of compositions (Ca/Si-ratio of 0.27-0.53, alkali/Si-ratio between 0.25-1.15) was analysed in [63]. A disc of gel in a cylinder with a disc of cement paste at the top and the bottom were placed in distilled water allowing capillary suction and diffusion by the cement paste discs. Free swelling was measured and a reverse swelling pressure was calculated. Unfortunately, it is not clear what the composition of the solution is that reaches the gel discs through the cement paste discs. If the ionic strength in the pore solution of the gel discs is higher than the one of the solution in the cement paste discs, osmotic swelling occurs. This seems to be the cause of swelling observed in these experiments. However, the relation between the concentration of ions in the solution present in ASR-affected aggregates and the surrounding cement paste is the opposite. The ion concentration in the pore solution of the cement paste is higher than in the solution present in the aggregate. This concentration gradient causes the diffusion of ions into the aggregate and is the pre-requisite for an on-going ASR.

These studies show that some amorphous ASR products are able to swell. However, it is not clear if this applies as well to the specific chemical boundary conditions present in concrete aggregates. Additionally, if ASR products are in contact with a liquid in concrete, it would be pore solution and not water. Therefore, any experiments exposing ASR products to water seem to be questionable. In any case, water uptake of ASR products in concrete can be expected to occur by vapour sorption. Experiments should take this into account. Moreover, the typical range of internal RH of concrete [64] and the one relevant for ASR have to be considered as well. The threshold of RH for ASR to occur is between 80 and 90 % [65-66]. In concrete structures, RH is fluctuating due to exposure to rain and changes in temperature, although this effect is usually restricted to the outermost centimetres of the concrete [67]. As a result, adsorption and desorption of water vapour and a possible volume change of amorphous ASR products can be expected. However, it is not clear if his process can cause expansion and stress. In the CPT, the RH is constant in the range of 93.5-96 % [68]. Obviously, fluctuations in RH are no prerequisite for concrete expansion.

It seems questionable, if bulk experiments on synthetic ASR products are able to simulate the processes taking place in reactive aggregates, as they so far are no able to take into account the complex ion transport along charged surfaces pointed out in paragraph 5.2.

5.4 Moisture stability of crystalline ASR products

So far, few data on the volume change of crystalline ASR products due to water vapour sorption exist. However, the drying of concrete samples and subsequent epoxy impregnation must cause a shrinkage of the crystalline ASR products present in aggregates with the formation of small cracks, as it can easily be seen in Figure 4.5. Additionally, this can be observed in the same experiment in the ESEM, as already described for amorphous ASR product (see paragraph 5.3). An increase of RH from 40 to 95 % leads to a decrease of crack width (Figure 5.2).

In a recent paper [43], the water vapour sorption of crystalline ASR products was determined (Figure 5.3). The samples sorbed 15-22 mass-% of water from 70 and 98 % RH. However, such a value can be reached solely by surface sorption without water uptake in the interlayer. Such a water uptake in the interlayer would cause an increase in d-value and would be the proof for the swelling of crystalline ASR products comparable to specific clays [69-73]. For the experiment, the three different crystalline ASR products formed in concrete exposed to natural environment were conditioned at 50 % RH before the first XRD measurement and at 100 % RH before the second measurement conducted in sealed capillaries. As it can be seen in Figure 5.4, there is no change in d-values between dry and moist state. These results were confirmed by [56] that showed no changes in d-value at RH values relevant for ASR by synchrotron-based in-situ 3D micro-XRD experiments. Additionally, synthesized crystalline ASR products (10.8 and 13.4 Å phase, see paragraph 4.2) show no increase in d-value upon water sorption

as well [3,27]. Consequently, swelling of crystalline ASR products due to water uptake in the interlayer is no cause for stress generation. This does not exclude that crystalline ASR products can contribute to stress generation by crystallisation pressure or as a contributor to mass accumulation in aggregates.

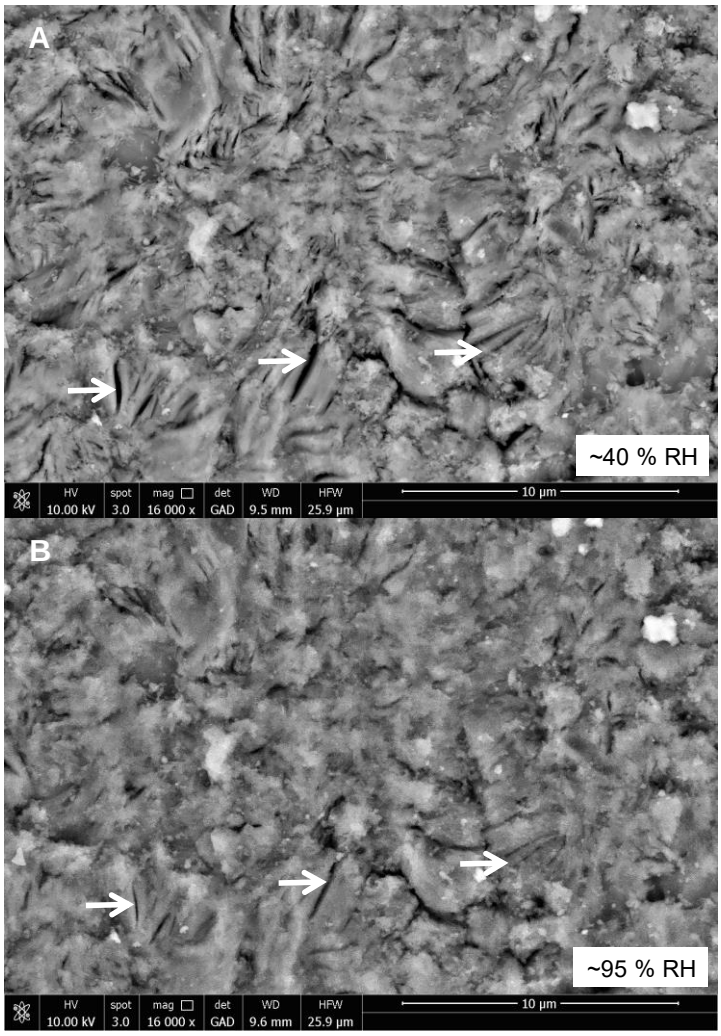

Figure 5.2: Ground concrete sample showing a vein in an aggregate filled with crystalline ASR product in the ESEM at ~ 40 (A) and ~ 95 (B) % RH. Figure 5.2A shows the sample at the beginning of the experiment before adsorption and Figure 5.2B was made on the desorption path after reaching the point of water condensation. The white arrows indicate locations with differences in crack width. HFW = 25.9 µm.

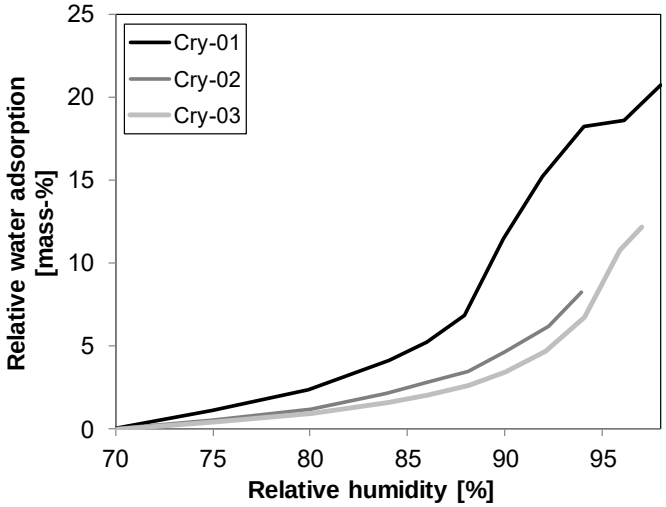

Figure 5.3: Dynamic vapour sorption (desorption) of crystalline ASR products formed in aggregates. Concrete from a bridge. Data from [43].

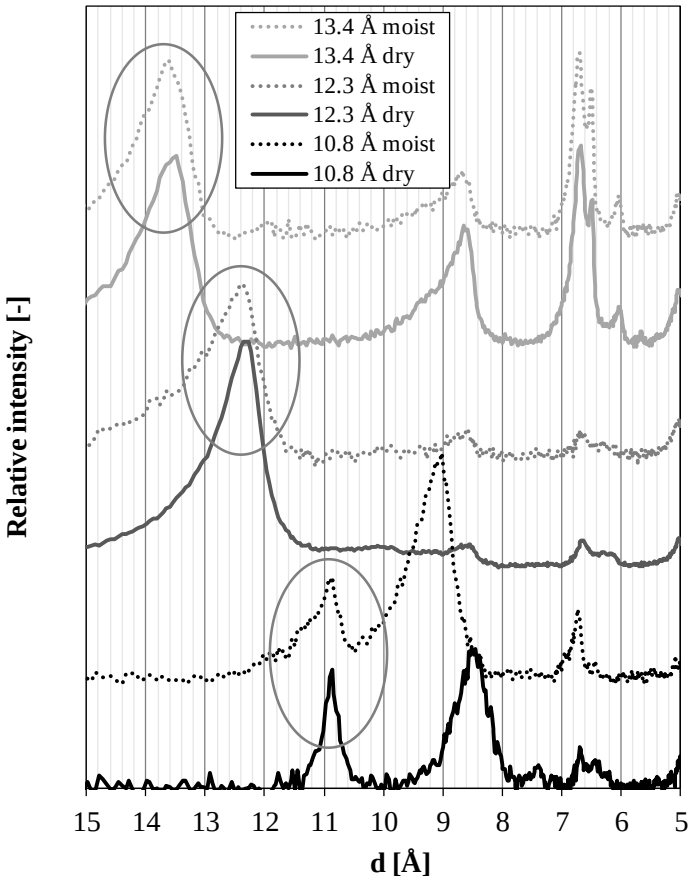

Figure 5.4: The d-spacing of the 10.8, 12.3 and 13.4 Å phases pre-conditioned at 50 ("dry") and 100 % RH ("moist") measured in a sealed capillary. The ellipses indicate the relevant reflections. Data from [43].

6. SUMMARY

The formation of amorphous ASR products starts in aggregates close to the interface with the cement paste followed by a continuous ingress towards the interior of the aggregates.

At the point of cracking, there is an immediate extrusion of ASR product into the cement paste, which leaves the majority of the cracks in aggregates empty.

After initial cracking, mostly crystalline ASR products start to fill the empty cracks in the aggregates again moving as a front from the edge of the aggregates inward.

The chemical composition of amorphous and crystalline ASR products is very similar in a mature state with values in atomic ratios of 0.20-0.35 for Ca/Si and 0.15-0.35 for (Na+K)/Si. The amorphous ASR products display a higher Na/K than the crystalline ones in non-boosted concrete.

The structure of the amorphous ASR product leading to the initial cracking of aggregates contains Q^3 sites (layers of SiO_2 tetrahedra) and Q^2 sites (chains of SiO_2 tetrahedra).

The crystalline ASR product formed in concrete displays a layer-silicate structure. Raman microscopy allows to distinguish between two different types and XRD between three different types with d-values of 10.8, 12.3 and 13.4 Å. The 13.4 Å phase is formed at high temperatures > 60 °C and corresponds to shlykovite. As shown by synthesis, the other two phases form at 20 (12.3 Å) and 40 °C (10.8 Å), respectively.

Mimicking the swelling of amorphous ASR products in laboratory conditions is challenging. However, the microstructural evidence clearly indicates that amorphous products are the cause of initial aggregate cracking.

XRD analysis of d-values in dry and moist conditions shows that none of the three identified types of crystalline ASR product sorb water in the interlayer between 50 and 100 % RH, excluding this mechanism as a reason of swelling and stress generation.

The mechanism for stress generation by ASR products remains unclear.

7. ACKNOWLEDGEMENTS

The author would like to thank Pietro Lura and Zhenguo Shi for stimulating discussions and for reviewing the manuscript.

8. REFERENCES

[1] Leemann A (2021) Impact of different added alkalis on concrete expansion due to ASR. In: Proceedings of the 16th ICAAR, Volume I, Lisbon, Portugal, pp 175-184

[2] Leemann A, Merz C (2013) An attempt to validate the ultra-accelerated microbar and the concrete performance test with the degree of AAR-induced damage observed in concrete structures. Cem Concr Res 49:29-37. https://doi.org/10.1016/j.cemconres.2013.03.014

[3] Shi Z, Geng G, Leemann A, Lothenbach B (2019) Synthesis, characterization, and water uptake property of alkali-silica reaction products. Cem Concr Res 121:58–71. https://doi.org/10.1016/j.cemconres.2019.04.009

[4] Leemann A, Shi Z, Lindgård J (2020) Characterization of amorphous and crystalline ASR products formed in concrete aggregates. Cem Concr Res 137:106190. https://doi.org/10.1016/j.cemconres.2020.106190

[5] Walther JV, Helgeson HC (1977) Calculation of the thermodynamic properties of aqueous silica and the solubility of quartz and its polymorphs at high pressures and temperatures. Am J Sci 277:1315–1351. https://doi: 10.2475/ajs.277.10.1315

[6] Iler RK (1979) The Chemistry of Silica: Solubility, Polymerization, Colloid and Surface Properties, and Biochemistry, Wiley, New York

[7] Willey JD (1980) Effects of aging on silica solubility: a laboratory study. Geochim Cosmochim Acta 44:573-578. https://doi.org/10.1016/0016-7037(80)90249-5

[8] Knauss KG, Wolery TJ (1988) The dissolution kinetics of quartz as a function of pH and time at 70 °C. Geochim Cosmochim Acta 52:43-53. https://doi.org/10.1016/0016-7037(88)90055-5

[9] Dove PM, Crerar DA (1990) Kinetics of quartz dissolution in electrolyte solutions using a hydrothermal mixed flow reactor. Geochim Cosmochim Acta 54:955-969. https://doi.org/10.1016/0016-7037(90)90431-J

[10] Varshneya AK (1994) Fundamentals of Inorganic Glasses, 2nd ed. Academic Press Inc, San Diego, CA

[11] Sjöberg S (1996) Silica in aqueous environments. J Non-Cryst Solids 196:51–57. https://doi.org/10.1016/0022-3093(95)00562-5

[12] Dove PM (1999) The dissolution kinetics of quartz in aqueous mixed cation solutions. Geochim Cosmochim Acta 63:3715-3727. https://doi.org/10.1016/S0016-7037(99)00218-5

[13] Brantley SL, Kubicki JD (2008) White AF Kinetics of Water–Rock Interaction. Springer, New York

[14] Rajabipour F, Giannini E, Dunant C, Ideker JH, Thomas MD (2015) Alkali–silica reaction: current understanding of the reaction mechanisms and the knowledge gaps. Cem Concr Res, 76, 130-146. https://doi.org/10.1016/j.cemconres.2015.05.024

[15] Bagheri M, Lothenbach B, Shakoorioskooie M, Scrivener K (2022) Effect of different ions on dissolution rates of silica and feldspars at high pH. Cem Concr Res 152:106644. https://doi.org/10.1016/j.cemconres.2021.106644

[16] Kawamura M (1998) Composition of ASR gels and expansion of mortars. In Materials Science of Concrete-Special Volume: The Sidney Diamond Symposium (pp. 261-276). American Ceramic Society

[17] Thaulow N, Jakobsen UH, Clark B (1996) Composition of alkali silica gel and ettringite in concrete railroad ties: SEM-EDX and X-ray diffraction analyses. Cem Concr Res 26(2):309-318. https://doi.org/10.1016/0008-8846(95)00219-7

[18] Katayama T (2012) Petrographic study of the alkali-aggregate reactions in concrete. PhD Thesis, University of Tokyo

[19] Leemann A, Katayama T, Fernandes I, Broekmans MA (2016) Types of alkali–aggregate reactions and the products formed. Proc Inst Civil Eng Constr Mater 169:128-135. https://doi.org/10.1680/jcoma.15.00059

[20] Guthrie GD, Carey JW (2015) A thermodynamic and kinetic model for paste–aggregate interactions and the alkali–silica reaction. Cem Concr Res 76:107-120. https://doi.org/10.1016/j.cemconres.2015.05.004

[21] Leemann A, Münch B (2019) The addition of caesium to concrete with alkali-silica reaction: Implications on product identification and recognition of the reaction sequence. Cem Concr Res 120:27-35. https://doi.org/10.1016/j.cemconres.2019.03.016

[22] Boehm-Courjault E, Leemann A (2017) Characterization of ASR products by SEM and TEM, Proc. 16th Euroseminar on Microscopy Applied to Building Materials, Les Diablerets, Switzerland

[23] Boehm-Courjault E, Barbotin S, Leemann A, Scrivener K (2020) Microstructure, crystallinity and composition of alkali-silica reaction products in concrete determined by transmission electron microscopy. Cem Concr Res, 130:105988. https://doi.org/10.1016/j.cemconres.2020.105988

[24] Shakoorioskooie M, Griffa M, Leemann A, Zboray R, Lura P (2021) Alkali-silica reaction products and cracks: X-ray micro-tomography-based analysis of their spatial-temporal evolution at a mesoscale. Cem Concr Res 150:106593. https://doi.org/10.1016/j.cemconres.2021.106593

[25] Münch B, Martin LH, Leemann A (2015) Segmentation of elemental EDS maps by means of multiple clustering combined with phase identification. J Microsc 260:411-426. https://doi.org/10.1111/jmi.12309

[26] Gaboriaud F, Nonat A, Chaumont D, Craievich A (1999) Aggregation and Gel Formation in Basic Silico-Calco-Alkaline Solutions Studied: A SAXS, SANS, and ELS Study. J Phys Chem B 103(28):5775-5781. https://doi.org/10.1021/jp990151s

[27] Shi Z, Leemann A, Rentsch D, Lothenbach B (2020) Synthesis of alkali-silica reaction product structurally identical to that formed in field concrete. Mater. Design 108562. https://doi.org/10.1016/j.matdes.2020.108562

[28] Shi Z, Park S, Lothenbach B, Leemann A (2020) Formation of shlykovite and ASR-P1 in concrete under accelerated alkali-silica reaction at 60 and 80 °C. Cem Concr Res137: 106213. https://doi.org/10.1016/j.cemconres.2020.106213

[29] Shi Z, Lothenbach B (2020) The combined effect of potassium, sodium and calcium on the formation of alkali-silica reaction products. Cem Concr Res 127:105914. https://doi.org/10.1016/j.cemconres.2019.105914

[30] Chatterji S, Jensen AD, Thaulow N, Christensen P (1986) Studies of alkali-silica reaction. Part 3. Mechanisms by which NaCl and $Ca(OH)_2$ affect the reaction. Cem Concr Res, 16:246-254. https://doi.org/10.1016/0008-8846(86)90141-9

[31] Wang H, Gillott JE (1991) Mechanism of alkali-silica reaction and the significance of calcium hydroxide. Cem Concr Res 21:647-654. https://doi.org/10.1016/0008-8846(91)90115-X

[32] Thomas M (2001) The role of calcium hydroxide in alkali recycling in concrete. Materials Science of Concrete Special, pp 225-236

[33] Fernandes I (2009) Composition of alkali-silica reaction products at different locations within concrete structures. Mater Charact 60:655-668. https://doi.org/10.1016/j.matchar.2009.01.011

[34] Katayama T, Drimalas T, Ideker JH, Fournier B (2012) ASR gels and their crystalline phases in concrete - universal products in alkali–silica, alkali–silicate and alkali–carbonate reactions. In Proceedings of the 14th ICAAR, Austin, Texas, pp 20-25

[35] Leemann A, Lura P (2013) E-modulus of the alkali-silica-reaction product determined by micro-indentation. Constr Build Mater 44:221-227. https://doi.org/10.1016/j.conbuildmat.2013.03.018

[36] Kirkpatrick RJ, Kalinichev AG, Hou X, Struble L (2005) Experimental and molecular dynamics modeling studies of interlayer swelling: water incorporation in kanemite and ASR gel. Mater Struct 38:449-458. https://doi.org/10.1007/BF02482141

[37] Hou X, Kirkpatrick RJ, Struble LJ, Monteiro PJ (2005) Structural investigations of alkali silicate gels. J Am Ceram Soc 88:943-949. https://doi.org/10.1111/j.1551-2916.2005.00145.x

[38] Benmore CJ, Monteiro PJ (2010) The structure of alkali silicate gel by total scattering methods. Cem Concr Res 40:892-897. https://doi.org/10.1016/j.cemconres.2010.02.006

[39] Leemann A (2017) Raman microscopy of alkali-silica reaction (ASR) products formed in concrete. Cem Concr Res 102:41-47. https://doi.org/10.1016/j.cemconres.2017.08.014

[40] Leemann A, Borchers I, Shakoorioskooie M, Griffa M, Müller Ch, Lura P (2019) Microstructural analysis of ASR in concrete – accelerated testing versus natural exposure. Proceedings pro128: International Conference on Sustainable Materials, Systems and Structures (SMSS2019). Durability, Monitoring and Repair of Structures. RILEM Publications S.A.R.L, Paris, France

[41] Kirkpatrick RJ, Yarger JL, McMillan PF, Ping Y, Cong X, (1997) Raman spectroscopy of CSH, tobermorite, and jennite. Adv Cem Mater 5:93-99. https://doi.org/10.1016/S1065-7355(97)00001-1

[42] Fernandes I, Leemann A, Fournier B, Menéndez E, Lindgård J, Borchers I, Custódio J (2022) PARTNER Project post documentation study – condition assessment of field exposure site cubes (Part II – results of microstructural analyses), Proceedings of the 16th ICAAR, Lisbon, Portugal, pp 385-386

[43] Leemann A, Shi Z, Wyrzykowski M, Winnefeld F (2020) Moisture stability of crystalline alkali-silica reaction products formed in concrete exposed to natural environment. Cem Concr Res 137: 106190. https://doi.org/10.1016/j.cemconres.2020.106190

[44] Buck AD, Mather K (1978) Alkali-Silica Reaction Products from Several Concretes: Optical, Chemical, and X-Ray Diffraction Data (No. WES-MP-C-78-7). ARMY ENGINEER WATERWAYS EXPERIMENT STATION VICKSBURG MISS

[45] Cole WF, Lancucki CJ, Sandy MJ (1981) Products formed in an aged concrete. Cem Concr Res 11:443–454. https://doi.org/10.1016/0008-8846(81)90116-2

[46] Cole WF, Lancucki CJ (1983) Products formed in an aged concrete the occurrence of okenite. Cem Concr Res 13:611–618. https://doi.org/10.1016/0008-8846(83)90049-2

[47] Berube MA, Fournier B, (1986) Les produits de la reaction alcalis-silice dans le beton; etude de cas de la region de Quebec. Can Mineral 24:271-288

[48] Shayan A, Lancucki CJ (1986) Alkali-aggregate reaction in the Causeway Bridge, Perth, western Australia, In: P.E. Grattan-Bellew (editor): Proceedings, 7th ICAAR, Ottawa, Canada: Concrete Alkali-Aggregate Reactions, Noyes Publications, Park Ridge, New Jersey, USA, pp 392-397

[49] De Ceukelaire L (1991) The determination of the most common crystalline alkali–silica reaction product. Mater Struct 24 169-171. https://doi.org/10.1007/BF02472981

[50] Jensen V. (1993) Alkali aggregate reaction in southern Norway. Doctor Technicae Thesis, Norwegian University of Science and Technology-NTNU, Trondheim/NO

[51] Marfil SA, Maiza PJ (2001) Deteriorated pavements due to the alkali–silica reaction: a petrographic study of three cases in Argentina. Cem Concr Res 31:1017–1021. https://doi.org/10.1016/S0008-8846(01)00508-7

[52] Peterson K, Gress D, van Dam T, Sutter L (2006) Crystallized alkali–silica gel in concrete from the late 1890s. Cem Concr Res 36.1523–1532, https://doi.org/10.1016/j.cemconres.2006.05.017

[53] Dähn R, Arakcheeva A, Schaub P, Pattison P, Chapuis G, Grolimund D, Wieland E, Leemann A (2016) Application of micro X-ray diffraction to investigate the reaction products formed by the alkali–silica reaction in concrete structures. Cem Concr Res 79:49–56. https://doi.org/10.1016/j.cemconres.2015.07.012

[54] Geng G, Shi Z, Leemann A, Borca C, Huthwelker T, Glazyrin K, ..., Wieland E (2020) Atomistic structure of alkali-silica reaction products refined from X-ray diffraction and micro X-ray absorption data. Cem Concr Res 129:105958. https://doi.org/10.1016/j.cemconres.2019.105958

[55] Geng G, Shi Z, Leemann A, Glazyrin K, Kleppe A, Daisenberger D, Churakov S, Lothenbach B, Dähn R, Wieland E (2020) Mechanical behavior and phase change of alkali-silica-reaction products under hydrostatic compression. Acta Crystallogr Sect B 76(4):674-682. https://doi.org/10.1107/S205252062000846X/rm5024sup1

[56] Geng G, Barbotin S, Shakoorioskooie M, Shi Z, Leemann A, Sanchez DF, Grolimund D, Wieland E, Dähn, R. (2021) An in-situ 3D micro-XRD investigation of water uptake by alkali-silica-reaction (ASR) product. Cem Concr Res 141:106331. https://doi.org/10.1016/j.cemconres.2020.106331

[57] Helmuth R, Stark D, Diamond S, Moranville-Regourd M (1993) Alkali-silica reactivity: an overview of research. Contract 100:202

[58] Barneyback Jr RS, Diamond S (1981) Expression and analysis of pore fluids from hardened cement pastes and mortars. Cem Concr Res 11:279-285. https://doi.org/10.1016/0008-8846(81)90069-7

[59] Lothenbach B, Winnefeld F (2006) Thermodynamic modelling of the hydration of Portland cement. Cem Concr Res 36:209-226. https://doi.org/10.1016/j.cemconres.2005.03.001

[60] Leemann A, Le Saout G, Winnefeld F, Rentsch D, Lothenbach B (2011) Alkali-silica reaction: the influence of calcium on silica dissolution and the formation of reaction products. J Am Ceram Soc 94:1243-1249. https://doi.org/10.1111/j.1551-2916.2010.04202.x

[61] Krough H (1975). Examination of synthetic alkali-silica gels. In: Proc Symp Alkali-Aggregate Reaction, pp 131-164

[62] Struble LJ, Diamond S (1981) Swelling properties of synthetic alkali silica gels. J Am Ceram Soc 64:652-655. https://doi.org/10.1111/j.1151-2916.1981.tb15864.x

[63] Gholizadeh-Vayghan A, Rajabipour F (2017) Quantifying the swelling properties of alkali-silica reaction (ASR) gels as a function of their composition. J Am Ceram Soc 100:3801-3818. https://doi.org/10.1111/jace.14893

[64] Parrott LJ (1991) Factors influencing relative humidity in concrete. Mag Concr Res 43:45-52. https://doi.org/10.1680/macr.1991.43.154.45

[65] Larive C, Laplaud A, Coussy O (2000) The role of water in alkali–silica reaction. In: Bérubé MA, Fournier B, Durand B (Eds.). 11th International Conference on Alkali–Aggregate Reaction, Québec, Canada, pp 61–69

[66] Jensen V (2004) Alkali–silica reaction damage to Elgeseter Bridge, Trondheim, Norway: a review of construction, research and repair up to 2003. Mater Charact 53:155-170. https://doi.org/10.1016/j.matchar.2004.09.006

[67] Rust CK (2009) Role of relative humidity in concrete expansion due to alkali-silica reaction and delayed ettringite formation: relative humidity thresholds, measurement methods, and coatings to mitigate expansion. Doctoral dissertation, University of Texas

[68] Lindgård J, Sellevold EJ, Thomas MD, Pedersen B, Justnes H, Rønning TF (2013) Alkali–silica reaction (ASR) - performance testing: influence of specimen pre-treatment, exposure conditions and prism size on concrete porosity, moisture state and transport properties. Cem Concr Res 53:145-167. https://doi.org/10.1016/j.cemconres.2013.05.020

[69] . Posner AM, Quirk JP (1964) Changes in basal spacing of montmorillonite in electrolyte solutions. J Colloid Interf Sci 19:798-812. https://doi.org/10.1016/0095-8522(64)90056-X

[70] Slade PG, Quirk JP, (1991) The limited crystalline swelling of smectites in $CaCl_2$, $MgCl_2$, and $LaCl_3$ solutions. J Colloid Interf Sci 144:18-26, https://doi.org/10.1016/0021-9797(91)90233-X

[71] Wangler T, Scherer GW (2008) Clay swelling mechanism in clay-bearing sandstones. Environ Geol 56:529-534. https://doi.org/10.1007/s00254-008-1380-3

[72] Anderson RL, Ratcliffe I, Greenwell HC, Williams PA, Cliffe S, Coveney PV (2010) Clay swelling - a challenge in the oilfield. Earth Sci Rev 98:201-216. https://doi.org/10.1016/j.earscirev.2009.11.003

[73] Tambach TJ, Bolhuis PG, Smit B (2004) A molecular mechanism of hysteresis in clay swelling. Angew Chem Int Ed 43:2650-2652. https://doi.org/10.1002/anie.200353612